# A one-step algorithm for spectral CT with an application on multi-source inverse geometry

Frédéric Jolivet, Clarisse Fournier, Jérôme Lesaint, Andrea Brambilla

# A one-step algorithm for spectral CT with an application on multi-source inverse geometry

Frédéric Jolivet, Clarisse Fournier, Jérôme Lesaint and Andrea Brambilla.

***Abstract*—Spectral computerized tomography (Spectral CT) is an imaging technique which uses the spectral information of the attenuated X-ray beam. Energy-resolved photon-counting detector is a promising technique for improved spectral CT imaging and allows to obtain material selective images. While energy-resolved photon-counting detectors can have good spectral resolution (with many energy bins), the size of these detectors is often limited. For their part Multi-Source Inverse Geometry CT (MS-IGCT) architectures allow the use of a smaller detector than conventional Cone Beam CT architecture (CBCT). In a previous work, we have proposed a one-step reconstruction algorithm validated with spectral data from classical Cone Beam CT architecture. In this work we propose to adapt this one-step method on spectral data from MS-IGCT architecture. From noisy simulated data, we compare the proposed one-step method with two two-step decomposition methods.**

***Index Terms*—Multi-source Inverse Geometry CT, Spectral CT, Iterative image reconstruction, Material decomposition.**

## I. Introduction

Spectral CT with energy-resolved photon-counting detectors gives the possibility to record the multi-energy data in a single acquisition [1]. One interest of spectral CT for medical x-ray imaging is to decompose the object onto some physical or materials basis [2]. Several approaches are proposed to tackle the decomposition problem. Two-step approaches first estimate multi-material decomposed sinograms from multi-energies sinograms. Then material specific images are reconstructed from the multi-material decomposed sinograms [3], [4]. One-step methods propose to tackle the decomposition problem in a one-step inversion, i.e. estimate multi-material reconstructions in the image domain from multi-energies sinograms [5], [6]. In a conventional CBCT architecture, the field of view of the reconstructed maps is directly limited by the size of the energy resolved photon counting detector. For their part multi-source inverse geometry CT (MS-IGCT) architectures (see Fig. 1 for example) allow the use of a smaller detector than conventional Cone Beam CT architecture [7]. Compared to conventional CBCT, MS-IGCT (with a small detector) also reduces scattered radiation, which should help improve material decomposition results. In previous works, we proposed an iterative tomographic reconstruction algorithm for MS-IGCT with an energy-integrating X-ray detector [8], and one-step method using photon-counting detectors for conventional CBCT architecture [9]. In this work, we adapt the one-step method [9] for multi-source inverse geometry CT and compare multi-material reconstructions obtained with the proposed method with those of two-step methods. The two-step methods estimate decomposed sinograms with a Maximum Likelihood Estimator (MLE), and from these decomposed sinograms the first two-step method uses Filtered Back-Projection (FBP) to obtain the multi-material reconstructions (in the image domain) whereas the second one uses a regularized tomographic reconstruction [8].

F. Jolivet is with the Univ. Grenoble Alpes, CEA, LETI, F-38000 Grenoble, France. E-mail: frederic.jolivet18@gmail.com .

J. Lesaint is with CEA, CTREG, DGDO, Bouguenais, France. (email : jerome.lesaint@cea.fr)

C. Fournier and A. Brambilla are with the Univ. Grenoble Alpes, CEA, LETI, F-38000 Grenoble, France. E-mail: firstname.lastname@cea.fr

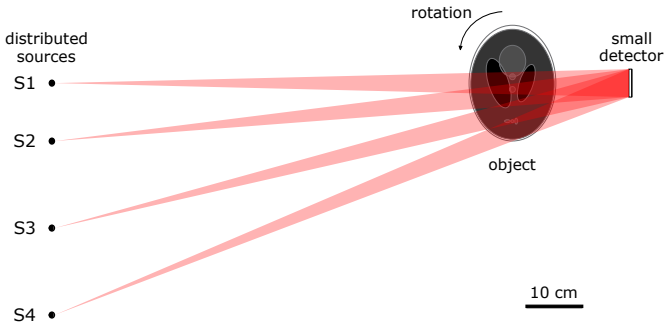


Fig. 1. Multi-Source Inverse Geometry setup.

## II. An Empirical imaging Model

In inverse problems approaches, the image formation model links the observed data to the imaged object according to the properties of the acquisition system and the unknown object. In spectral CT the energy-dependant attenuation coefficient is classically expressed as a linear combination of a few basis materials [2], [10]. This model combined with the forward model of spectral tomographic reconstruction (including the incident spectrum and the spectral response of the detector) leads to a non-convex optimization problem (in the inverse problems framework) [3], [6] and requires an accurate knowledge of the system response. In this work, we choose to use an empirical imaging model based on a linear fit of attenuation calibration data [4] and adapt it for multi-source inverse geometry architectures.

A calibration basis of two materials is used to determine the coefficients $p$ that best fits measurements obtained with $N$ combinations of material specific thicknesses. With multi-source inverse geometry, $N$ calibrated measurements are acquired for the energy-bin $c$ of the pixel $k$ when the $q$-th source is active. These measurements are collected in the vector $\boldsymbol{s}_{q,k,c}$,

$$\boldsymbol{s}_{q,k,c} = \boldsymbol{H}\boldsymbol{p}_{q,k,c} + \boldsymbol{e}^{calib}_{q,k,c} \tag{1}$$

where $\boldsymbol{s}_{q,k,c} \in \mathbb{R}^N$ and $\boldsymbol{e}^{calib}_{q,k,c} \in \mathbb{R}^N$ are respectively the calibration data vector and the error vector, whereas $\boldsymbol{p}_{q,k,c}$ is

a vector of two order-1-polynomial coefficients (in this work the number of basis materials is equal to 2) and $\boldsymbol{H} \in \mathbb{R}^{N\times 2}$ is a matrix defined by,

$$\boldsymbol{H} = \begin{pmatrix} l_{1,1} & \cdots & l_{1,N} \\ l_{2,1} & \cdots & l_{2,N} \end{pmatrix}^T .$$

Considering all vectors $\boldsymbol{e}_{q,k,c}^{calib}$ as white gaussian noises, we determine the coefficients $\boldsymbol{p}_{q,k,c}$ of these polynomial functions with,

$$\hat{\boldsymbol{p}}_{q,k,c} = \underset{\boldsymbol{p}\in\mathbb{R}^2}{\operatorname{argmin}} \|\boldsymbol{H}\boldsymbol{p} - \boldsymbol{s}_{q,k,c}\|_2^2 \tag{2}$$

The optimization problem (2) leads to the following closed-form solution (see chap.4 of the book [11]),

$$\hat{\boldsymbol{p}}_{q,k,c} = \left(\boldsymbol{H}^T\boldsymbol{H}\right)^{-1}\boldsymbol{H}^T\boldsymbol{s}_{q,k,c} \quad . \tag{3}$$

We use the coefficients $\hat{\boldsymbol{p}}_{q,k,c}$ to model the $C$ energy bins attenuation measurements at pixel $k$ and object rotation angle $\theta$ when the $q$-th source is active,

$$m_{q,k,\theta}(\boldsymbol{x}_1, \boldsymbol{x}_2) = \boldsymbol{M}_{q,k}\boldsymbol{\chi}_{q,k,\theta} \tag{4}$$

where $\boldsymbol{x}_1 \in \mathbb{R}^{N_x}$ (respectively $\boldsymbol{x}_2 \in \mathbb{R}^{N_x}$) is the material-specific sinogram for the material 1 (respectively for the material 2). The matrix $\boldsymbol{M}_{q,k} \in \mathbb{R}^{C\times 2}$ and the vector $\boldsymbol{\chi}_{q,k,\theta} \in \mathbb{R}^2$ are defined by,

$$\boldsymbol{M}_{q,k} = \begin{pmatrix} \hat{\boldsymbol{p}}_{q,k,1} & \cdots & \hat{\boldsymbol{p}}_{q,k,C} \end{pmatrix}^T \quad \text{and} \quad \boldsymbol{\chi}_{q,k,\theta} = \begin{pmatrix} [\boldsymbol{x}_1]_{q,k,\theta} \\ [\boldsymbol{x}_2]_{q,k,\theta} \end{pmatrix},$$

where $[\boldsymbol{x}_\eta]_{q,k,\theta} = [\boldsymbol{A}\boldsymbol{z}_\eta]_{q,k,\theta}$ with $\boldsymbol{A}$ the forward projection matrix and $\boldsymbol{z}_\eta$ is the vector of $N_z$ unknowns in the image domain for the material $\eta$.
This leads to the following data formation model,

$$\boldsymbol{d}_{q,k,\theta} = m_{q,k,\theta}(\boldsymbol{x}_1, \boldsymbol{x}_2) + \boldsymbol{e}_{q,k,\theta} \tag{5}$$

where $\boldsymbol{d}_{q,k,\theta} \in \mathbb{R}^C$ is the data vector for the $k$-th pixel of the $\theta$-th object rotation angle when the $q$-th source is active and $\boldsymbol{e}_{q,k,\theta} \in \mathbb{R}^C$ is the error vector including different noises (detection noise, modeling noise...).
Note : In conventional CBCT, it is crucial to have pixel-specific model (and therefore a pixel-specific calibration) to take into account the non-uniform response between each pixels detector. In MS-IGCT, we must also take into account the variation between each sources.

## III. The proposed one-step method

Considering all error vectors $\boldsymbol{e}_{q,k,\theta}$ in (5) are Gaussian noises, the data fidelity term can be formulated as the negative log-likelihood,

$$\mathcal{F}(\boldsymbol{x}_1, \boldsymbol{x}_2) = \sum_{q=1}^{Q}\sum_{k=1}^{K}\sum_{\theta=1}^{\Theta} \|m_{q,k,\theta}(\boldsymbol{x}_1, \boldsymbol{x}_2) - \boldsymbol{d}_{q,k,\theta}\|^2_{\boldsymbol{W}_{q,k}} \tag{6}$$

with $\boldsymbol{W}_{q,k}$ the inverse of the covariance matrix of the noise for the $k$-th pixel when the $q$-th source is active (in our case $\boldsymbol{W}_{q,k}$ is diagonal because we assume a non correlated noise), $K$ is the number of detector pixels, $\Theta$ is the number of object rotation angles and $Q$ is the number of sources. This inverse problem is ill-posed and ill-conditioned. For this reason it is necessary to introduce prior information in order to restrict ambiguity for the inversion. In inverse problems framework, these prior information can be termed as a feasibility set (bound constraints,...) and/or a regularization function to favor specific properties of the spatial distribution of the reconstructed object. In our case we assume an isotropic total variation regularization which promotes piecewise-constant objects [12], [13] on reconstruction objects $\{\boldsymbol{z}_1, \boldsymbol{z}_2\}$, and a feasible set $\Omega$. The proposed one-step method for MS-IGCT can be formulated as an optimization problem,

$$\hat{\boldsymbol{z}} \in \underset{\boldsymbol{z}}{\operatorname{argmin}}\ \mathcal{F}(\boldsymbol{A}\boldsymbol{z}_1, \boldsymbol{A}\boldsymbol{z}_2) + \mathcal{R}(\boldsymbol{z}_1, \boldsymbol{z}_2) \tag{7}$$

where $\boldsymbol{z} = \begin{pmatrix} \boldsymbol{z}_1 \\ \boldsymbol{z}_2 \end{pmatrix}$ and $\mathcal{R}$ is a regularization term which introduces an isotropic total variation constraint in the image domain and could restrict $\boldsymbol{z}$ values to a feasible set $\Omega$ (a non-negativity constraint for instance). Thus $\mathcal{R}$ is defined by

$$\mathcal{R}(\boldsymbol{z}_1, \boldsymbol{z}_2) = \lambda\sum_{\eta=1}^{2} \|\nabla\boldsymbol{z}_\eta\|_{2,1} + i_{\boldsymbol{z}\in\Omega}(\boldsymbol{z}_1, \boldsymbol{z}_2) \quad , \tag{8}$$

where $i_{\boldsymbol{z}\in\Omega}$ is the indicator function which restrict $\boldsymbol{z}$ values to the set $\Omega$, $\lambda \in \mathbb{R}^+$ is an hyperparameter that balances the weight of the regularization term with the data fidelity term and $\|.\|_{2,1}$ is the (2,1)-mixed norm $\ell_{2,1}$.

## IV. Proposed iterative reconstruction algorithm

In the previous section we have formulated the inverse problem as the large scale optimization problem (7) which is non-smooth (due to the regularization term). Furthermore, the data fidelity and the regularization term are not in the same domain, respectively in the projection domain and the image domain. For these reasons the optimization problem (7) is challenging. In order to limit the time complexity of the reconstruction, it is important to solve data fidelity term in the projection domain. We therefore choose to use a variable splitting strategy such that at convergence $\boldsymbol{x}_\eta = \boldsymbol{A}\boldsymbol{z}_\eta$. We reformulate the optimization problem (7) as the following constrained optimization problem,

$$\hat{\boldsymbol{z}} \in \underset{\substack{\boldsymbol{x},\boldsymbol{z} \\ \text{s.t. } \boldsymbol{x}=\tilde{\boldsymbol{A}}\boldsymbol{z}}}{\operatorname{argmin}}\ \mathcal{F}(\boldsymbol{x}_1, \boldsymbol{x}_2) + \mathcal{R}(\boldsymbol{z}_1, \boldsymbol{z}_2) \tag{9}$$

where $\boldsymbol{x} = \begin{pmatrix} \boldsymbol{x}_1 \\ \boldsymbol{x}_2 \end{pmatrix}$ and $\tilde{\boldsymbol{A}} = \boldsymbol{I}_2 \otimes \boldsymbol{A}$ with $\boldsymbol{I}_2$ is the identity matrix and $\otimes$ is the Kronecker product. The function $\mathcal{F}(\boldsymbol{x}_1, \boldsymbol{x}_2)$ is smooth convex, and $\mathcal{R}(\boldsymbol{z}_1, \boldsymbol{z}_2)$ is a non-smooth and non-linear function. To handle the constrained optimization problem (9), we can form the augmented Lagrangian $\mathcal{L}_\rho$ and search for a saddle point,

$$\begin{aligned}\mathcal{L}_\rho(\boldsymbol{x}, \boldsymbol{z}, \boldsymbol{u}) = \mathcal{F}(\boldsymbol{x}_1, \boldsymbol{x}_2) + \mathcal{R}(\boldsymbol{z}_1, \boldsymbol{z}_2) \\ + \rho\sum_{\eta=1}^{2}\left(\|\boldsymbol{x}_\eta - \boldsymbol{A}\boldsymbol{z}_\eta + \boldsymbol{u}_\eta\|_2^2 - \|\boldsymbol{u}_\eta\|_2^2\right)\end{aligned} \tag{10}$$

where $\boldsymbol{u}_{\eta=1,2} \in \mathbb{R}^{N_x}$ are the scaled dual variables, and $\rho \in \mathbb{R}^+$ is the augmented Lagrangian penalization parameter [14]. To find a saddle point we can resolve alternatively

a minimization with respect to the primal variables and a maximization with respect to the dual variables,

$$\left\{\boldsymbol{x}^{(j+1)}, \boldsymbol{z}^{(j+1)}\right\} \in \underset{\boldsymbol{x},\boldsymbol{z}}{\operatorname{argmin}}\ \mathcal{L}_{\rho}(\boldsymbol{x}, \boldsymbol{z}, \boldsymbol{u}^{(j)})$$
$$\text{dual update}: \boldsymbol{u}_{\eta}^{(j+1)} = \boldsymbol{u}_{\eta}^{(j)} + \boldsymbol{x}_{\eta}^{(j+1)} - \boldsymbol{A}\boldsymbol{z}_{\eta}^{(j+1)}$$

where $\eta \in \{1, 2\}$ and $(j)$ corresponds to the iteration number. This optimization problem can be performed by the Alternating Direction Method of Multipliers (ADMM) [14],

$$\boldsymbol{x}^{(j+1)} = \underset{\boldsymbol{x}}{\operatorname{argmin}}\ \mathcal{L}_{\rho}\left(\boldsymbol{x}, \boldsymbol{z}^{(j)}, \boldsymbol{u}^{(j)}\right) \tag{11}$$
$$\boldsymbol{z}^{(j+1)} = \underset{\boldsymbol{z}}{\operatorname{argmin}}\ \mathcal{L}_{\rho}\left(\boldsymbol{x}^{(j+1)}, \boldsymbol{z}, \boldsymbol{u}^{(j)}\right) \tag{12}$$
$$\boldsymbol{u}_{\eta}^{(j+1)} = \boldsymbol{u}_{\eta}^{(j)} + \boldsymbol{x}_{\eta}^{(j+1)} - \boldsymbol{A}\boldsymbol{z}_{\eta}^{(j+1)}, \forall\ \eta \in \{1, 2\}\,.$$

Since the projection matrix $\boldsymbol{A}$ is a linear operator, the minimization problem (12) is a convex/non-smooth large-scale optimization problem solved with the MS-IGCT reconstruction method [8]. On the other hand, the minimization problem (11) is a convex/smooth minimization problem which is separable and can thus be solved independently pixel by pixel and source by source with the following closed-form expression,

$$\widehat{\boldsymbol{\chi}}_{q,k,\theta}^{(j+1)} = (\boldsymbol{M}_{q,k}^{T}\boldsymbol{W}_{q,k}\boldsymbol{M}_{q,k} + \rho\boldsymbol{I}_2)^{-1}(\boldsymbol{M}_{q,k}^{T}\boldsymbol{W}_{q,k}\boldsymbol{d}_{q,k,\theta} + \rho\boldsymbol{v}_{q,k,\theta}^{(j)}),$$

with $\boldsymbol{I}_2$ the identity matrix and $\boldsymbol{v}_{q,k,\theta} = \begin{pmatrix}[\boldsymbol{A}\boldsymbol{z}_1 - \boldsymbol{u}_1]_{q,k,\theta} \\ [\boldsymbol{A}\boldsymbol{z}_2 - \boldsymbol{u}_2]_{q,k,\theta}\end{pmatrix}$. The closed-form solution of (11) is the key point of the proposed one-step method.

## V. Experiments & Results

### A. Simulations

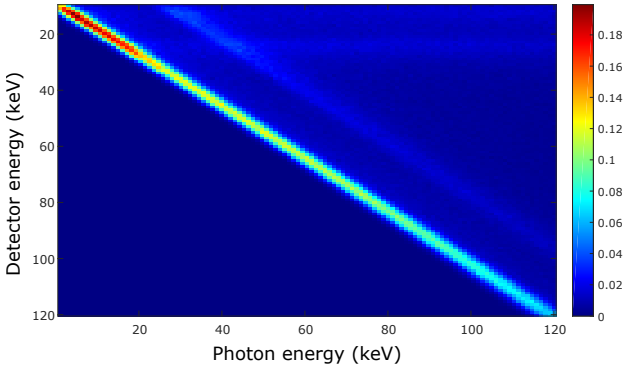


Fig. 2. Detector Response Matrix for the simulated CdTe detector.

Fig. 1 is a realistic illustration of the simulated MS-IGCT architecture. We simulate 4 distributed sources shifted from 0 to 40 cm (0/10/25/40cm). The source-to-detector distance is 100 cm whereas the source-to-isocenter distance is 80 cm. The object is a Shepp-Logan Phantom of $18.4\times13.8$ cm, containing different proportions of water and cortical bone materials. The simulated photon counting detector is a line of 50 pixels with a pitch of $1 \times 1\ mm^2$ (i.e. detector size $\sim 5$ cm). The detector is simulated with one hundred and eleven energy bins from 10keV to 120keV and the realistic Detector Response Matrix (DRM) shown in Fig. 2. The simulated source was set to 140kV with 0.1 cm aluminum filtration at 0.1 mA.s per projection which result of an x-ray exposure of $5\times10^6$ photons per pixel. Attenuation coefficients of water and cortical bone come from the computer program XMuDat [15]. Energy-resolved photon counting data are corrupted by a Poissonnian noise. These simulated data are represented Fig.3. A two basis material calibration of water and cortical bone was simulated with 15 thicknesses ranging from 0 to 17 cm for the water, and 15 thicknesses ranging from 0 to 6 cm for the cortical bone.

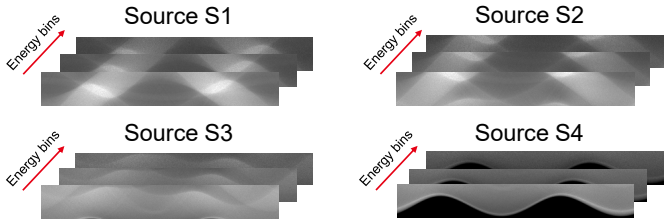


Fig. 3. Truncated simulated sinograms of the MS-IGCT architecture (Fig.1).

### B. Results

Fig. 4 shows a comparison between 3 methods : the proposed one-step method (fourth column) with a non-negativity constraint. **Method 1** (second column) : A two-step method based on a Maximum Likelihood Estimation (MLE) of materials sinograms $\boldsymbol{x}$ (which consists in minimizing the data fidelity expressed in (6) ) followed by a filtered back-projection step. **Method 2** (third column) : A two-step method based on the same first step but followed by a regularized tomographic reconstruction method with TV regularization adapted for MS-IGCT [8]. For the last method, regularization hyperparameters of the second step are tuned automatically to maximize reconstruction's Peak Signal-to-Noise Ratio (PSNR). All these reconstructions are obtained from simulated data described in Sec. V-A and can be compared with ground truth (second column). Results in Fig. 4 show that the proposed one-step method gives reconstructions with a better PSNR than the two-step methods (see Tab.I). Regarding the proposed one-step method, the number of iterations needed to solve (12) is another key parameter to maximize the ratio reconstruction image quality vs. computation time. In our case, 15 iterations of the regularized reconstruction for MS-IGCT [8] give satisfying reconstructions. To finish we applied 50 iterations of the ADMM method. The proposed method is implemented on GPU to drastically reduce the computational time.

| PSNR | Method 1 | Method 2 | Proposed method |
|---|---|---|---|
| Bone | 18.05 dB | 23.31 dB | 29.66 dB |
| Water | 11.15 dB | 22.25 dB | 23.30 dB |

TABLE I
Reconstruction's Peak-Signal-to-Noise Ratio.

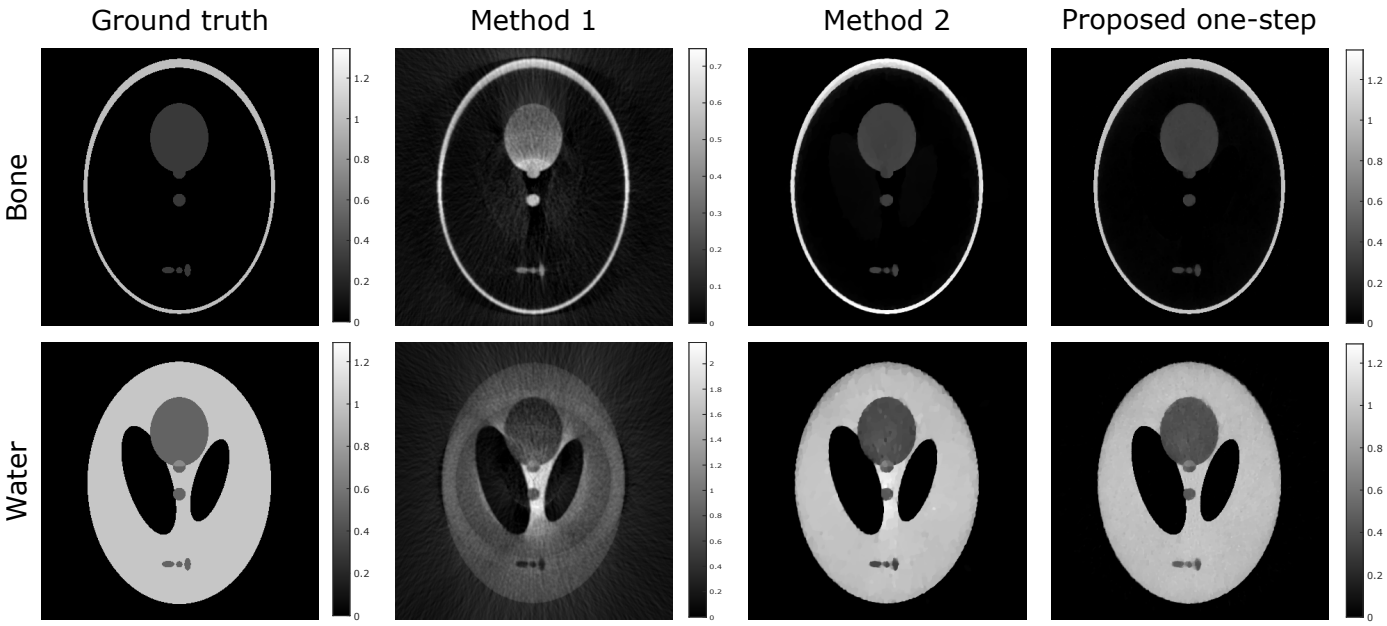


Fig. 4. Comparison of bone (top) and water (bottom) reconstructions in the image domain with spectral data from MS-IGCT architecture with 4 distributed sources and a small detector (5 cm). The ground truth (first column), and reconstructions obtained with the two-step method based on MLE decomposed sinograms followed by regularized iterative reconstructions (third column) and reconstructions obtained with the proposed one-step method (fourth column). With an other corlorbar, reconstructions obtained with the two-step based on MLE decomposed sinograms followed by filtered back-projections (second column).

## VI. Conclusion & Perspectives

We have proposed a one-step method which has been applied on spectral data for a multi-source inverse geometry CT. This one step method used an empirical model based on calibration data, and an alternating optimization strategy. The data fidelity reconstruction step is solved with a closed-formed expression, which drastically reduces the computation time of the material decomposition. The total-variation constraint and bound constraints are introduced by the iterative regularized reconstruction method for multi-source inverse geometry [8]. The present work shows that the proposed method reduces the noise for a bi-material reconstruction. Finally, this work opens up interesting perspectives for spectral CT reconstruction with a small spectral detector and a flat panel of sources. These preliminary - but promising - results, obtained on noisy simulated data, must now be validated on experimental spectral data.

## Acknowledgment

We acknowledge the financial support of the Cross-Disciplinary Program on Instrumentation and Detection of CEA, the French Alternative Energies and Atomic Energy Commission.

## References

[1] K. Taguchi and J. S. Iwanczyk, "Vision 20/20: Single photon counting x-ray detectors in medical imaging," *Medical physics*, vol. 40, no. 10, 2013.

[2] R. E. Alvarez and A. Macovski, "Energy-selective reconstructions in x-ray computerised tomography," *Physics in Medicine & Biology*, vol. 21, no. 5, p. 733, 1976.

[3] N. Ducros, J. F. P.-J. Abascal, B. Sixou, S. Rit, and F. Peyrin, "Regularization of nonlinear decomposition of spectral x-ray projection images," *Medical physics*, vol. 44, no. 9, pp. e174–e187, 2017.

[4] R. E. Alvarez, "Estimator for photon counting energy selective x-ray imaging with multibin pulse height analysis," *Medical physics*, vol. 38, no. 5, pp. 2324–2334, 2011.

[5] C. Mory, B. Sixou, S. Si-Mohamed, L. Boussel, and S. Rit, "Comparison of five one-step reconstruction algorithms for spectral ct," *Physics in Medicine & Biology*, vol. 63, no. 23, p. 235001, 2018.

[6] R. F. Barber, E. Y. Sidky, T. G. Schmidt, and X. Pan, "An algorithm for constrained one-step inversion of spectral ct data," *Physics in Medicine & Biology*, vol. 61, no. 10, p. 3784, 2016.

[7] B. De Man, S. Basu, P. Fitzgerald, D. Harrison, M. Iatrou, K. Khare, J. LeBlanc, B. Senzig, C. Wilson, Z. Yin *et al.*, "Inverse geometry ct: The next-generation ct architecture?" in *2007 IEEE Nuclear Science Symposium Conference Record*, vol. 4. IEEE, 2007, pp. 2715–2716.

[8] F. Jolivet, C. Fournier, and A. Brambilla, "A fast gradient-based algorithm for image reconstruction in inverse geometry ct architecture with sparse distributed sources," in *15th International Meeting on Fully Three-Dimensional Image Reconstruction in Radiology and Nuclear Medicine*, vol. 11072. International Society for Optics and Photonics, 2019, p. 110721N.

[9] F. Jolivet, J. Lesaint, C. Fournier, M. Garcin, and A. Brambilla, "An efficient one-step method for spectral ct based on an approximate linear model," *IEEE Transactions on Radiation and Plasma Medical Sciences*, 2020.

[10] J. P. Schlomka, E. Roessl, R. Dorscheid, S. Dill, G. Martens, T. Istel, C. Bäumer, C. Herrmann, R. Steadman, G. Zeitler *et al.*, "Experimental feasibility of multi-energy photon-counting k-edge imaging in pre-clinical computed tomography," *Physics in Medicine & Biology*, vol. 53, no. 15, p. 4031, 2008.

[11] S. M. Kay, *Fundamentals of statistical signal processing*. Prentice Hall PTR, 1993.

[12] L. I. Rudin, S. Osher, and E. Fatemi, "Nonlinear total variation based noise removal algorithms," *Physica D: nonlinear phenomena*, vol. 60, no. 1-4, pp. 259–268, 1992.

[13] A. Chambolle, "An algorithm for total variation minimization and applications," *Journal of Mathematical imaging and vision*, vol. 20, no. 1-2, pp. 89–97, 2004.

[14] S. Boyd, N. Parikh, E. Chu, B. Peleato, J. Eckstein *et al.*, "Distributed optimization and statistical learning via the alternating direction method of multipliers," *Foundations and Trends® in Machine learning*, vol. 3, no. 1, pp. 1–122, 2011.

[15] R. Nowotny, "Xmudat: Photon attenuation data on pc," *IAEA Report IAEA-NDS*, vol. 195, 1998.